scientific reports

OPEN

Endolymphatic hydrops and cochlear synaptopathy after noise exposure are distinct sequelae of hair cell stereociliary bundle trauma

Michelle L. Fong[1,6], Connie B. Paik[1,6], Patricia M. Quiñones[1], Clayton B. Walker[1,2], Michael J. Serafino[1], Dorothy W. Pan[1], Eduardo Martinez[1], Juemei Wang[1], Grady W. Phillips[3], Brian E. Applegate [1,4], Michael Anne Gratton[5] & John S. Oghalai [1,4✉]

Endolymphatic hydrops, increased endolymphatic fluid within the cochlea, is the key pathologic finding in patients with Meniere's disease, a disease of episodic vertigo, fluctuating hearing loss, tinnitus, and aural fullness. Endolymphatic hydrops also can occur after noise trauma and its presence correlates with cochlear synaptopathy, a form of hearing loss caused by reduced numbers of synapses between hair cells and auditory nerve fibers. Here we tested whether there is a mechanistic link between these two phenomena by using multimodal imaging techniques to analyze the cochleae of transgenic mice exposed to blast and osmotic challenge. In vivo cochlear imaging after blast exposure revealed dynamic increases in endolymph that involved hair cell mechanoelectrical transduction channel block but not the synaptic release of glutamate at the hair cell–auditory nerve synapse. In contrast, ex vivo and in vivo auditory nerve imaging revealed that synaptopathy requires glutamate release from hair cells but not endolymphatic hydrops. Thus, although endolymphatic hydrops and cochlear synaptopathy are both observed after noise exposure, one does not cause the other. They are simply co-existent sequelae that derive from the traumatic stimulation of hair cell stereociliary bundles. Importantly, these data argue that Meniere's disease derives from hair cell transduction channel blockade.

Keywords Hearing, Cochlea, Auditory nerve, Hair cell, Osmosis, Optical coherence tomography

Approximately 15% of Americans have hearing loss due to noise exposure[1]. The classical explanation is trauma to the cochlear hair cells, which begins when the hair cell stereociliary bundles transduce the mechanical energy of sound into electro-chemical signals. Because they are highly mechanosensitive, the hair bundles are easily damaged by loud sounds. Through a variety of pathways[2,3], hair cell death occurs causing permanent hearing loss evidenced by elevated auditory thresholds. An additional mechanism of noise-induced hearing loss that can occur without hair cell death is cochlear synaptopathy[4]. The postulated mechanism of cochlear synaptopathy is the excess release of glutamate, the hair cell afferent neurotransmitter, occurs with hair cell overstimulation or after extracellular ATP released from other traumatized cells activates Ca^{2+} channels[5,6]. This results in the toxic entry of ions and water into synaptic boutons[7–9] which damages the dendrite and produces loss of synaptic ribbons in residual hair cells[10–12]. Loss of auditory neurons does not necessarily elevate the threshold of hearing but instead affects neural encoding at higher sound intensities, and so it has been called "hidden" hearing loss[13]. There are no effective treatments used clinically to prevent hearing loss via either mechanism after traumatic noise exposure. Cochlear synaptopathy is likely to be a common form of hearing loss in humans[4,14].

[1]Caruso Department of Otolaryngology – Head and Neck Surgery, University of Southern California, Los Angeles, CA 90033, USA. [2]Department of Biomedical Engineering, Texas A&M University, College Station, TX 77843, USA. [3]Department of Otolaryngology – Head and Neck Surgery, Washington University in St. Louis, St. Louis, MO 63130, USA. [4]Department of Biomedical Engineering, University of Southern California, Los Angeles, CA 90089, USA. [5]Center for Sensory Neuroscience, Boys Town National Research Hospital, Omaha, NE 68010, USA. [6]Michelle L. Fong and Connie B. Paik: These two authors contributed equally to this work. ✉email: oghalai@usc.edu

To study this phenomenon, we have been exposing mice to damaging levels of sound using blast or noise and performing live imaging of their inner ears using optical coherence tomography (OCT)[15–17]. We found that endolymphatic hydrops develops prior to cochlear synaptopathy and hair cell loss. This is a build-up of endolymphatic fluid within the scala media chamber of the cochlea, the hallmark pathologic finding in Meniere's disease, a disabling syndrome of episodic vertigo, fluctuating hearing loss, and aural fullness with no known etiology[18–20]. Interestingly, the threshold level of noise needed to produce endolymphatic hydrops is identical to that needed to develop cochlear synaptopathy (bandpass filtered white noise > 95 dB)[17]. Also, applying hypertonic saline to draw H_2O out of the endolymph both treats the endolymphatic hydrops and reduces the loss of cochlear synapses. Together, these data suggest that endolymphatic hydrops might cause cochlear synaptopathy. To investigate this hypothesis, we used transgenic mouse models lacking either hair cell stereociliary bundle stimulation (Tecta$^{C1509G/C1509G}$)[21–23] or glutamate release (Vglut3^{KO})[24,25]. We compared blast exposure versus hypotonic challenge, an experimental technique that causes endolymphatic hydrops without damaging cochlear mechanics[15,26]. We found that both key findings of Meniere's disease, endolymphatic hydrops and cochlear synaptopathy, are distinct yet co-existent sequelae that derive from hair cell stereociliary bundles trauma.

Results

The development of endolymphatic hydrops after blast exposure requires stereociliary bundle stimulation but not glutamate release at the synapse

Our noise exposure protocol for this study was a blast wave, as opposed to continuous noise exposure, because it offers several benefits. For example, a single blast insult at a defined time is applied, allowing the investigator to immediately begin assessing the sequence of damage that results. In comparison, cochlear damage during continuous noise exposure accumulates during the time of the exposure, and early effects can be missed. Furthermore, the blast wave is applied only to one anesthetized mouse at a time while it is held by a pouch in such a way that the ears are in a consistent orientation. This improves the repeatability of the exposure over awake mice in a cage, which can sometimes have one or both ears covered by other mice or by bedding material.

We have previously shown that wild-type (WT) mice develop both stereociliary trauma and endolymphatic hydrops after blast trauma[15]. However, we found that stereociliary bundles in Tecta$^{C1509G/C1509G}$ mice are not damaged by the blast, presumably because they are not connected to the tectorial membrane. Also, they do not develop endolymphatic hydrops. This was a key line of evidence underlying our hypothesis that WT mice develop endolymphatic hydrops because their stereociliary bundles are damaged by the blast. This would block transduction channels, resulting in an increase in endolymph $[K^+]$, with the increased osmotic load pulling H_2O from the perilymph into the endolymph. Thus, we thought it likely that transduction channel block was the sole cause of endolymphatic hydrops.

To support this interpretation, we first wanted to test whether another key aspect of hair cell function that would be affected by the blast exposure, the synaptic release of glutamate, was involved in the development of endolymphatic hydrops. Therefore, we exposed Vglut3^{KO} mice to the blast wave. Vglut3^{KO} mice have normal hair cell mechanoelectrical transduction but they do not have glutamate synaptic release[27]. We imaged the apical turn of the cochlea using OCT (Fig. 1). The scala media and scala vestibuli cross-sectional areas were individually segmented and the scala media/scala vestibuli area ratio was used to assess the volume of endolymph quantitatively. Like wild-type mice, we found that Vglut3^{KO} mice developed endolymphatic hydrops after blast exposure, as shown by a statistically significant increase in SM/SV ratio between control ($n = 5$) and blast-exposed ($n = 7$) mice (Fig. 2, unpaired t-test, $t(10) = 2.33$, $p < 0.05$). These data indicate that glutamate release at the synapse is not involved in the development of endolymphatic hydrops.
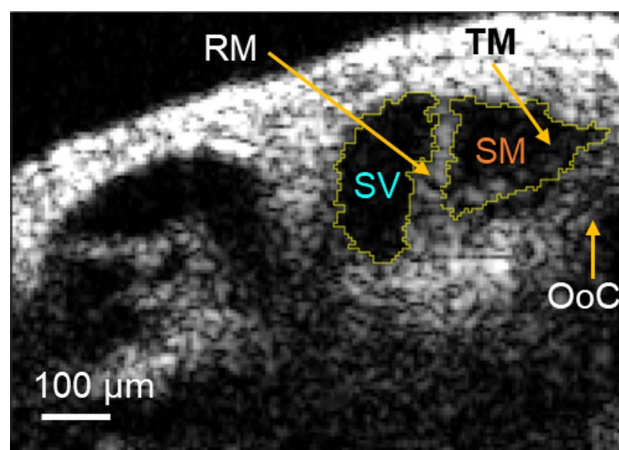
Fig. 1. The ratio of the cross-sectional areas of scala media to scala vestibuli was used to quantify endolymph volume. SM = Scala Media, SV = Scala Vestibuli, RM = Reissner's Membrane, TM = Tectorial Membrane, OoC = Organ of Corti.
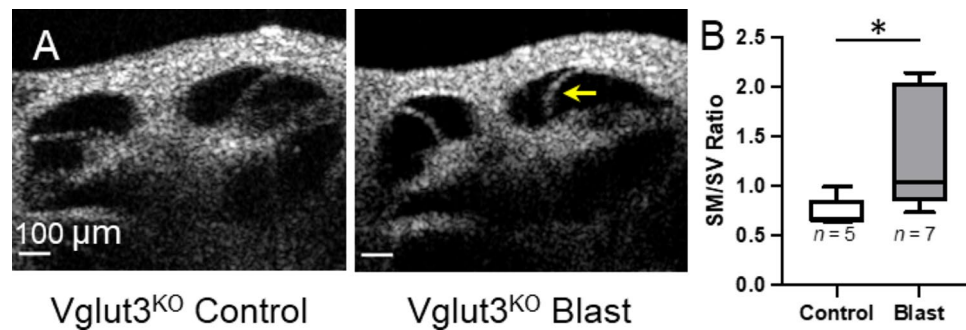
Fig. 2. Endolymph volume increases after blast exposure in the Vglut3[KO] mouse. (**A**) OCT visualization of the apical turn of the cochlea in a control mouse not exposed to blast (*left*) and a mouse three hours after blast exposure (*right*). Endolymphatic hydrops could be noted after blast by distension of Reissner's membrane (*arrow*). (**B**) The SM to SV area ratio significantly increased after blast exposure, indicating endolymphatic hydrops. *p < 0.05.

Endolymphatic hydrops occurs due to transduction channel block

To determine if transduction channel block alone is enough to cause endolymphatic hydrops, we perfused the perilymph with UoS-7692, a MET channel blocker known to provide more than 70% block of the MET current at 50 μM (Kenyon et al., 2021). We found that wild-type mice developed endolymphatic hydrops after exposure to UoS-7692 (Fig. 3A-A"), but not after injection of vehicle alone (0.2% DMSO in artificial perilymph) (Fig. S1A-A"). Quantification of the SM/SV ratio showed an increase after UoS-7692 injection over 300 min that was statistically significant (Fig. 3B n = 5, paired t-test, t(4) = 3.03, p < 0.05). Infusion of the vehicle control did not change the SM/SV ratio (Fig. S1B, $n = 3$).

To verify that this was related to transduction channel blockade, we measured basilar membrane vibratory responses to sound stimuli. As would be expected if OHCs no longer detected the sound input and thus could not amplify the traveling wave, the vibratory tuning curves turned from active (Fig. 3C) to passive (Fig. 3C'-C") after injection of UoS-7692. There was a reduction in the gain (Fig. 3D, n = 5, paired t-test, t(4) = 8.22, p < 0.01), and a shift in the CF to lower frequencies (Fig. 3E) at 90 and 180 min ($n = 5$, paired t-test, t(4) = 6.67, p < 0.01) that further decreased at 300 min ($n = 5$, paired t-test, t(4) = 8.92, p < 0.001). After vehicle control infusion, vibrometry curves, gain, and CF did not change. These data indicate that MET channel block is sufficient to cause endolymphatic hydrops.

Endolymphatic hydrops is due to an osmotic gradient between perilymph and endolymph

Application of a hypotonic challenge to the round window membrane causes endolymphatic hydrops in wild-type mice[15]. We wanted to determine whether this challenge, like blast exposure, occurred due to an effect on hair cell transduction. Thus, we applied hypotonic challenge to the round window of wild-type, *Tecta*[C1509G/C1509G], and Vglut3[KO] mice to test whether either of the two key features of hair cells, stereociliary bundle transduction and glutamate synaptic release, are required (Fig. 4). Wild-type mice developed endolymphatic hydrops after 30 min and 60 min ($n = 7$, paired t-test, t(6) = 3.43, p < 0.05) as did Vglut3[KO] mice ($n = 7$, paired t-test, t(6) = 4.67, p < 0.01). A mild case of endolymphatic hydrops existed in the *Tecta*[C1509G/C1509G] mice SM prior to the challenge, likely due to the partial closure of the transduction channels due to the lack of a deflection bias on the hair cell bundles[23]. However, after the challenge, the SV volume increased indicating the greater presence of endolymphatic hydrops ($n = 6$, paired t-test, t(5) = 4.09, p < 0.01) in the *Tecta*[C1509G/C1509G] mice.

As controls, we applied normotonic artificial perilymph to the round window membrane. As expected, there was no change in the scala media/scala vestibuli area ratio in wild-type or Vglut3[KO] mice (Fig. S2). Together, these findings argue that the position of Reissner's membrane simply reflects the osmotic load of the endolymph relative to the perilymph and does not necessarily involve hair cells.

Cochlear synaptopathy after blast exposure requires hair cell glutamate release

Next, we sought to understand the relationship between endolymphatic hydrops and cochlear synaptopathy. Wild-type, *Tecta*[C1509G/C1509G], and Vglut3[KO] mice were exposed to a blast wave to determine the role of hair cell stereociliary bundle stimulation and glutamate release on the development of cochlear synaptopathy. Mice were then housed for eight days before harvesting their inner ears and immunolabeling whole mount preparations to count pre-synaptic ribbons and post-synaptic densities (Fig. 5). Control mice were of equal age but not exposed to the blast wave.

First, we compared baseline counts between the genotypes (Fig. S3). As has been previously reported[28], we confirmed that the number of baseline pre-synaptic ribbons and post-synaptic densities per IHC is reduced across the cochlea in Vglut3[KO] mice ($n = 10$, ANOVA, F(2,61) = 185.7, p < 0.001; post-hoc Tukey, p < 0.001). This supports the concept that glutamate plays a role in synapse maintenance. We also found that *Tecta*[C1509G/C1509G] mice had fewer pre-synaptic ribbons per IHC at baseline in the apical and middle regions of the cochlea (~ 12–15 vs. ~ 15–20; $n = 5$–10, ANOVA; post-hoc Tukey, p < 0.05).

Next, we assessed the effect of blast exposure. As expected, wild-type mice developed synaptopathy[15]. When quantified, there was a significant decrease in the number of pre-synaptic ribbons per IHC across all
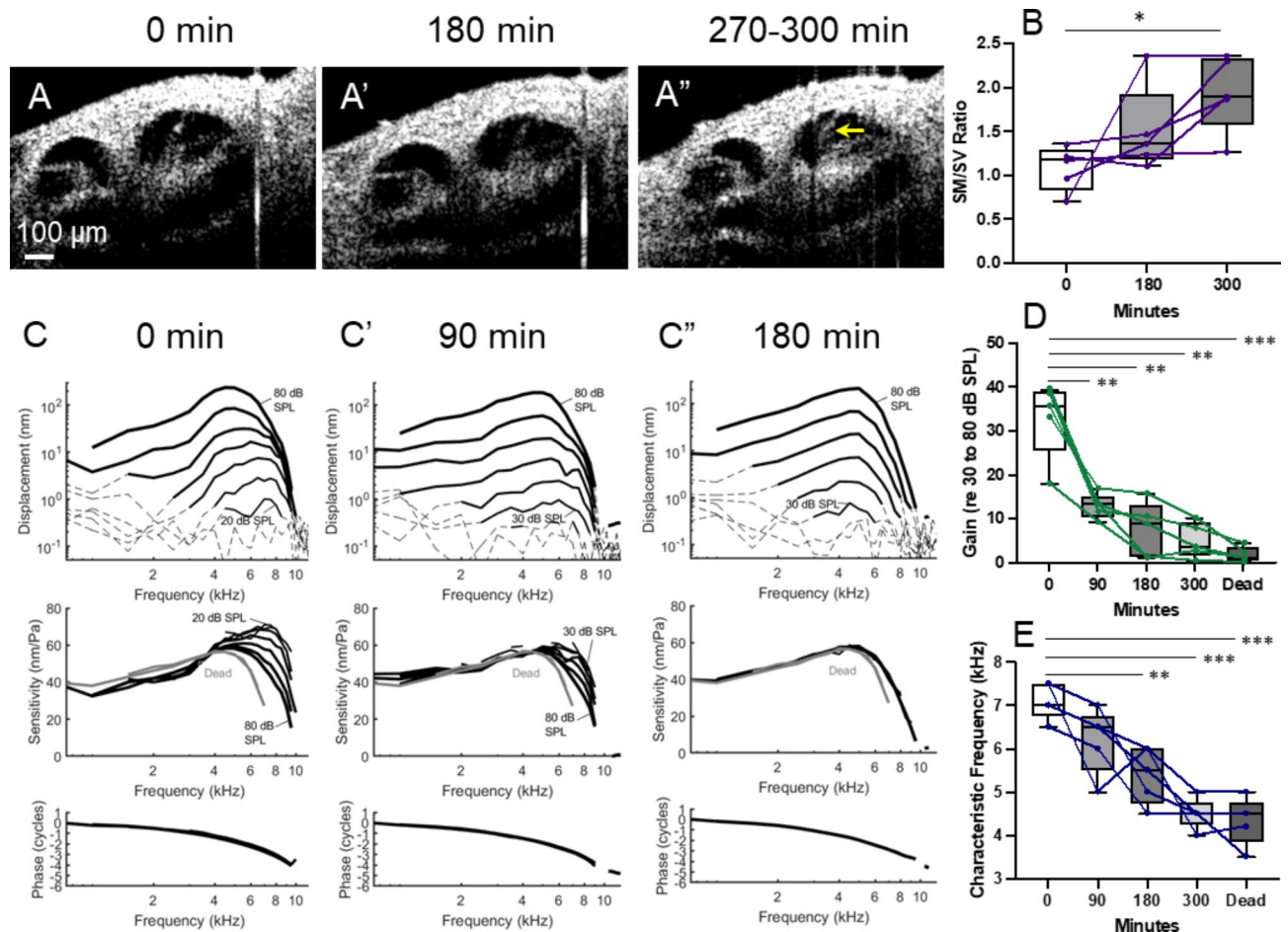
Fig. 3. Perilymphatic perfusion of the MET channel blocker UoS-7692 in wild-type mice causes loss of cochlear amplification and endolymphatic hydrops. (**A-A"**) OCT visualization of the cochlea apical turn at baseline 0 min (prior), 180 min, and 270–300 min after PSCC injection of UoS-7692 in one representative mouse. (**B**) The SM to SV ratio increases after MET channel blockade. (**C–C"**) Basilar membrane vibration demonstrates loss of cochlear amplification in the representative mouse during the experiment. This is best seen in the middle row of curves, where the sensitivity plots all overlap each other in C". (**D**) Cochlear gain and (**E**) characteristic frequency shift downward after MET channel blocker injection, and reach purely passive, post-mortem levels. *p < 0.05, **p < 0.01, ***p < 0.001, n = 5.

sections of the cochlea between controls (n = 10) and blast (n = 4) (Fig. 6A, Table S1, ANOVA, F(2,44) = 27.2, p < 0.0001; post-hoc Tukey, p < 0.05). The number of post-synaptic densities per IHC also decreased when comparing controls (n = 10) to blasts (n = 4) but the difference was only significant in the basal section of the cochlea (Fig. 6A', ANOVA, F(2,44) = 13.2, p < 0.0001; post-hoc Tukey, p < 0.05). There was no difference in pre-synaptic ribbons or post-synaptic densities after blast exposure in *Tecta*[C1509G/C1509G] (Fig. 6B-B', Table S1) or Vglut3[KO] mice (Fig. 6C-C', Table S1). These data indicate that while stereociliary bundle stimulation is necessary for synaptopathy to occur following a blast wave, it is insufficient without glutamate release from the hair cell.

Endolymphatic hydrops and cochlear synaptopathy do not always co-exist but both findings reflect osmotic fluid shifts

Next, we sought to determine if a hypotonic challenge that causes endolymphatic hydrops also causes cochlear synaptopathy. Wild-type, *Tecta*[C1509G/C1509G], and Vglut3[KO] mice were given a hypotonic challenge by applying distilled H$_2$O to the round window membrane of their right cochlea for 5.5 h. As described earlier, all three mouse strains demonstrated endolymphatic hydrops during this hypotonic challenge. We counted pre-synaptic ribbons and post-synaptic densities eight days later. For all three strains of mice, there were no significant differences in the number of pre-synaptic ribbons or post-synaptic densities across all regions of the cochlea after hypotonic challenge as compared to controls (Fig. 6, Table S2).

Thus, while this hypotonic challenge was sufficient to produce endolymphatic hydrops, it was insufficient to produce cochlear synaptopathy. To understand this, we first wanted to verify our expectation that the dendrites become swollen after blast trauma. We harvested cochleae and fixed them at 3, 7, and 24 h after blast exposure then acquired TEM micrographs to assess the ultrastructure of the hair cell – auditory nerve dendrite region. Representative images are shown (Figs. 7, S4). In control images, the diameter of a nerve fiber approximates 1 μm,
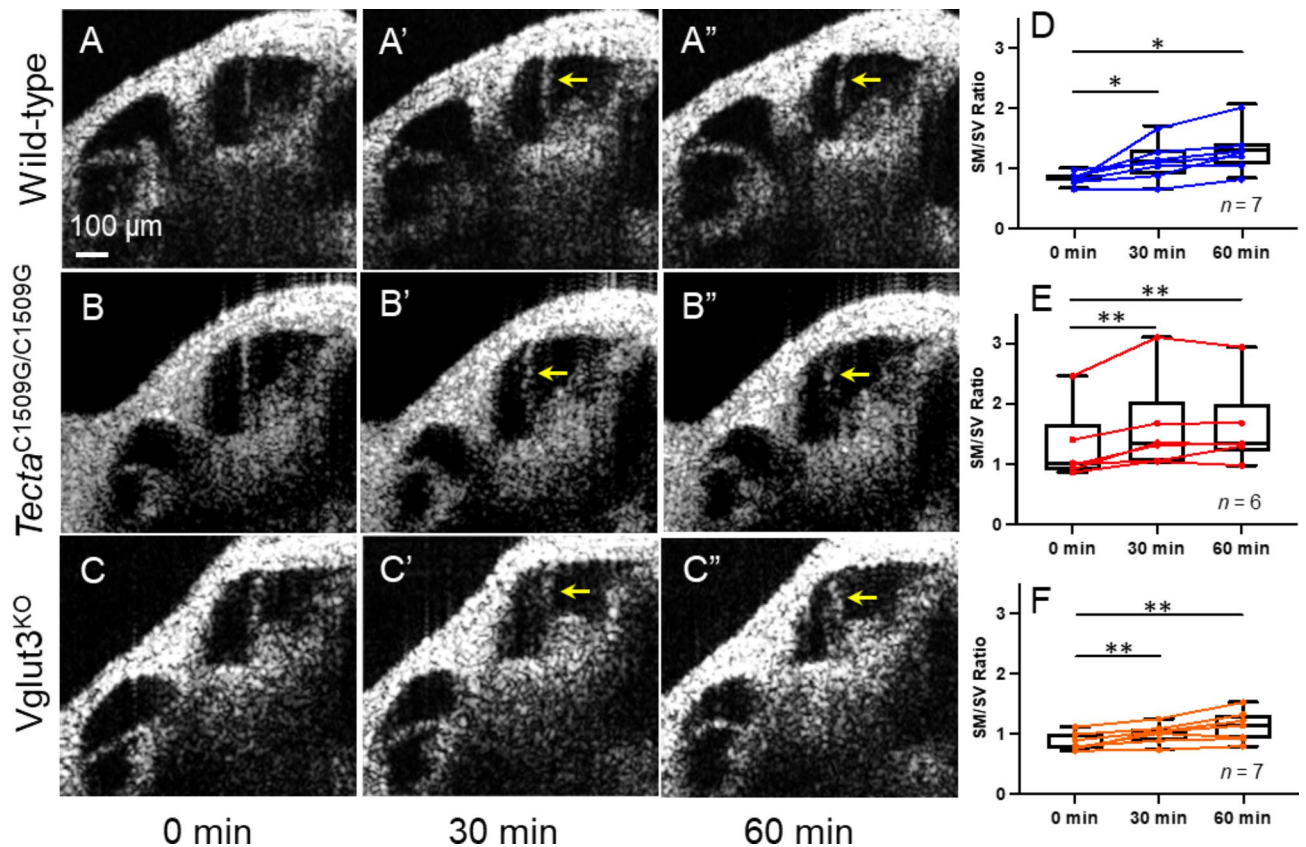
Fig. 4. Endolymph volume increases after hypotonic challenge in three different mouse models. OCT visualization of the apical turn of the cochlea in (**A-A"**) wild-type, (**B-B"**) $Tecta^{C1509G/C1509G}$, and (**C–C"**) Vglut3^{KO} mice at 0 min, 30 min, and 60 min after application of distilled water to the round window. The SM to SV ratio increases at 30 and 60 min after the application in (**D**) wild-type, (**E**) $Tecta^{C1509G/C1509G}$, and (**F**) Vglut3^{KO} mice. *p < 0.05, **p < 0.01.

which is consistent with the literature[29]. At 3, 7, and 24 h after a blast exposure, the dendrites swell, and nerve fiber diameter increases. Furthermore, there were additional ultrastructural changes consistent with metabolic stress after blast exposure such as tissue retraction, increased extracellular space, and reduced cytoplastic density of nerve fibers.

Osmotic effects within the cochlea occur very rapidly and also reverse within minutes[15]. Therefore, we did not perform electron microscopy imaging after hypotonic challenge because we were concerned that the fixation process would not be able to adequately capture the tissue at different time points. Thus, to validate these findings and compare blast-exposure versus hypotonic challenge, we measured dendritic diameter in vivo. We used two-photon microscopy to image through the round window of anesthetized Atoh1$^{CreERT2-tdTomato}$;Tau^{EGFP} mice (Fig. 8A-C). Synaptic boutons under the OHCs were easiest to analyze because of their scarcity, relative to the tightly packed boutons under the IHCs.

We verified that these were boutons from type II afferent dendrites and not medial olivocochlear efferent terminals by imaging at a plane in which the dendrites could be seen traveling longitudinally along the basal region of the three rows of OHCs (Fig. S5). Efferent nerves, while often visible crossing the tunnel of Corti in our images, do not have this innervation pattern when they reach the OHCs. Their synapses are a little higher up the lateral wall of the OHCs and there is no longitudinal travel (Spoendlin, 1985).

The boutons from the type II afferents were analyzed by measuring the width of their fluorescence intensity profile (Fig. 8D-F). Bouton diameter increased over four hours in the blast-exposed mice but did not change in control mice (Fig. 9A,B). The slope was 0.35 ± 0.21 μm/h for blast-exposed mice compared to -0.01 ± 0.04 μm/h for control mice, which was statistically different ($n = 5$, ANCOVA, $F(1,34) = 4.86$, p < 0.05). Similarly, bouton diameter increased over four hours in mice exposed to hypotonic challenge (0.258 ± 0.06 SEM μm/h, $n = 5$) but did not change in control mice (-0.01 ± 0.04 μm/h, $n = 5$), which also was statistically significant (Fig. 9C,D, ANCOVA, $F(1,43) = 13.39$, p < 0.01). We interpret these findings to indicate that although dendritic swelling occurs after both a blast exposure and hypotonic challenge, hypotonic challenge is not as severe and thus is reversible. This difference in severity is also consistent with different mechanisms causing the dendritic swelling, i.e., glutamate toxicity and free radical oxidation with blast but simple osmosis with hypotonic challenge.
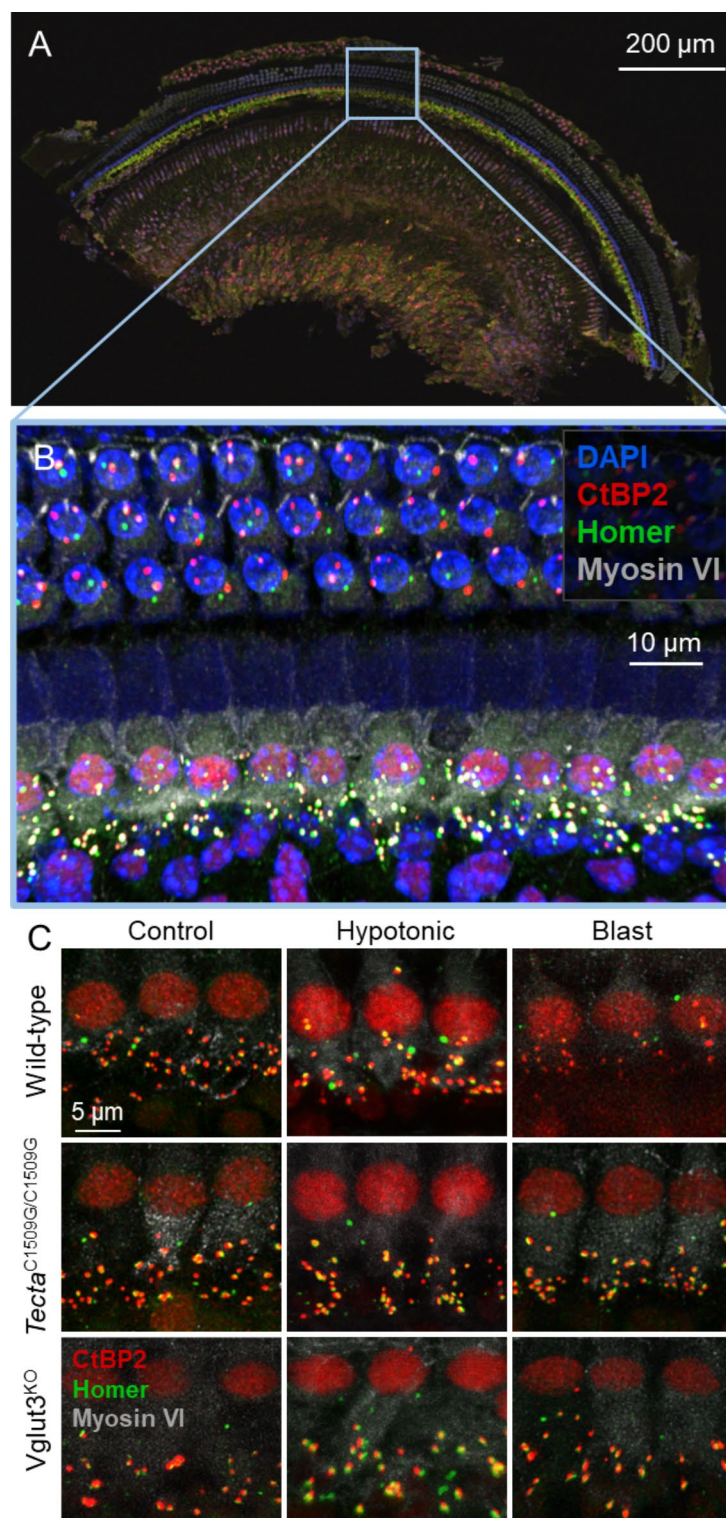
Fig. 5. Cochlear sections were imaged using confocal microscopy to assess for synaptic loss. (**A**) A middle cochlear section at $25\times$ magnification and (**B**) the region of interest for analysis at $63\times$ magnification. (**C**) Wild-type, $Tecta^{C1509G/C1509G}$, and Vglut3^{KO} mice were imaged 8 days after no exposure, hypotonic challenge, or blast exposure. Immunostaining was used to visualize hair cell nuclei (DAPI, *blue*), IHC nuclei and presynaptic ribbons (CtBP2, *red*), postsynaptic densities (Homer, *green*), and IHC bodies (myosin VI, *grey*).
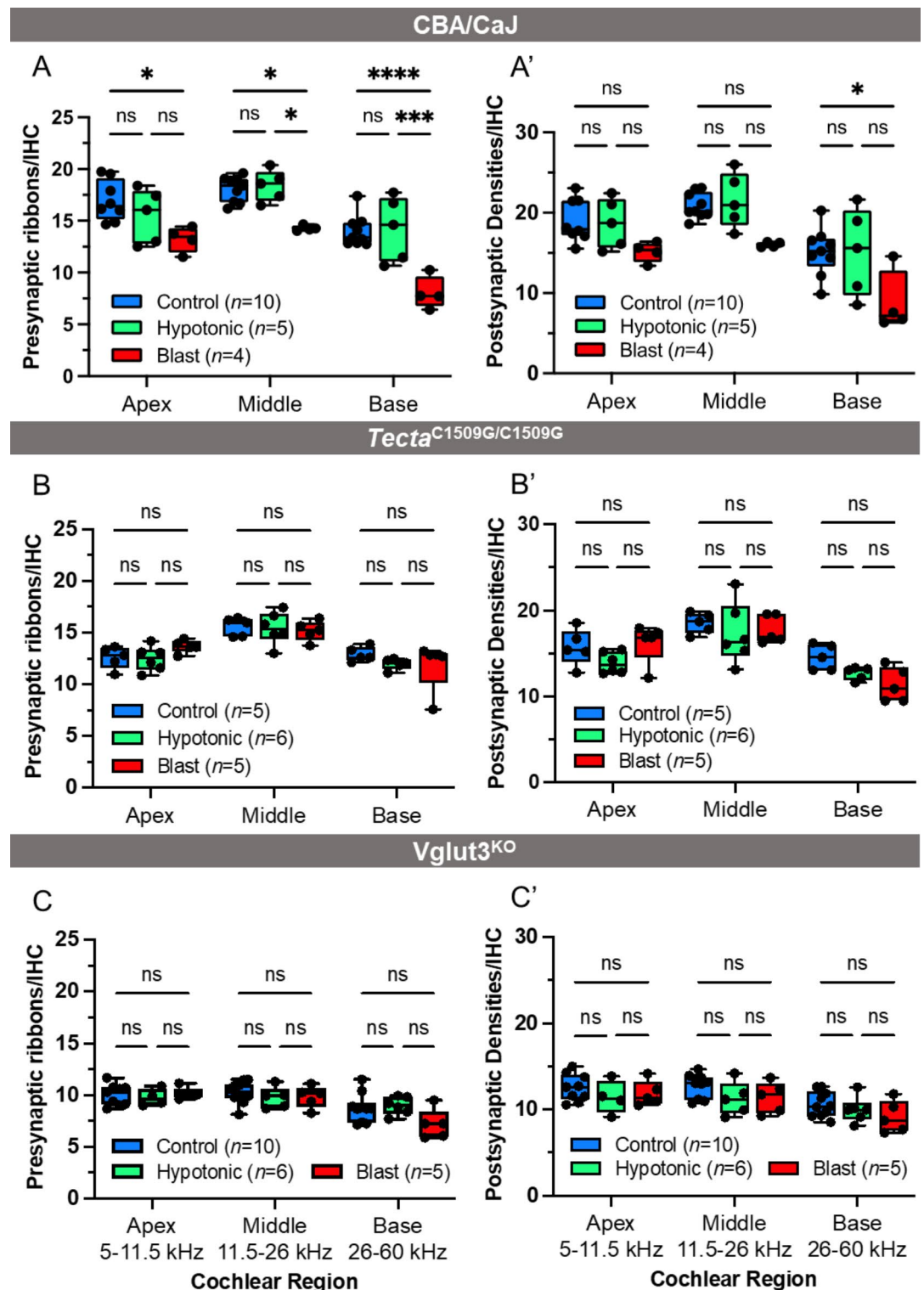
Fig. 6. Blast exposure causes a decrease in presynaptic ribbons and postsynaptic densities in wild-type mice only; hypotonic challenge has no significant effect on counts in any of the mouse strains. (**A-A'**) In wild-type mice, a blast exposure causes a significant decrease in the number of presynaptic ribbons across all regions of the cochlear, but only a significant loss of postsynaptic densities in the basal region. (**B-B', C–C'**) Presynaptic ribbon and postsynaptic density counts in *Tecta*^C1509G/C1509G and Vglut3^KO mice did not change after hypotonic challenge or blast exposure, indicating that the mutations in these mice eliminate crucial steps in the synaptopathy pathway. *p < 0.05, ***p < 0.001, ****p < 0.0001.
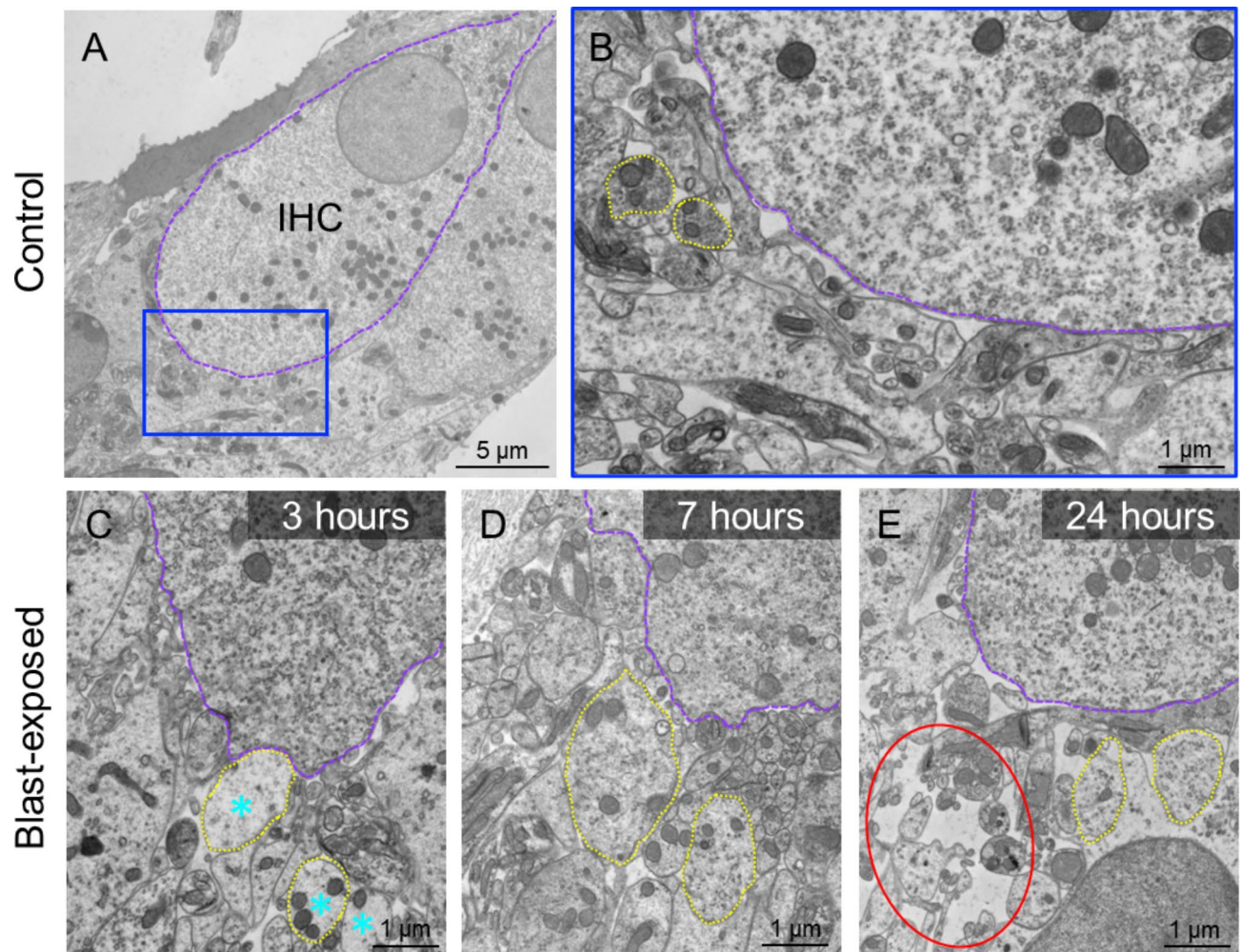
Fig. 7. Ultrastructural changes after a blast wave illustrated through TEM images of IHCs and synapse area. (**A**) Image of an IHC from a control mice taken at $1500\times$ magnification. (**B**) High power view of the region in the blue box from (*A*). (**C–E**) High-power views of representative blast-exposed mice harvested at 3, 7, and 24 h post-exposure. Individual dendrites outlined in yellow appear larger in area after blast exposure compared to control dendrites. *Cyan asterisks*: swollen dendrites with reduced cytoplasmic density. *Red ellipse*: increased extracellular space. All high-power images were taken at 6000x.

Discussion

Loud noise exposure produces a sense of fullness in the ear. This reflects endolymphatic hydrops and can result in permanent hearing loss due to cochlear synaptopathy and in some cases, hair cell damage. Here, we show that although endolymphatic hydrops and cochlear synaptopathy are both observed after blast exposure, endolymphatic hydrops does not cause synaptopathy. They are simply co-existent sequelae that both derive from the traumatic stimulation of hair cell stereociliary bundles. Our data, together with our previous publications[15,17] demonstrate that damage to the bundle closes the transduction channels, blocks the standing ionic current, and increases the osmotic load of the endolymph. This draws in H_2O from the perilymph and produces endolymphatic hydrops. Since blast trauma is complex and multifaceted, we cannot rule out the concept that other effects of the blast, such as hair cell or supporting cell rupture, may play a role too. However, the data presented here prove that MET channel blockade alone is sufficient to cause endolymphatic hydrops.

Similarly, overstimulation of the bundles leads to excess glutamate release which opens Na^+ channels in the dendrite, draws in H_2O and produces dendritic swelling, and results in cochlear synaptopathy. Furthermore, our data argue that the blast wave does not alter the conditions within the cochlea to the detriment of the auditory nerve by any means other than by stimulating hair cells to over-secrete glutamate. Thus, noise trauma does not directly alter the osmolarity of the intracochlear fluid compartment. This effect requires hair cell involvement.

Our synapse counts confirm and extend many previous findings from other labs. Importantly, the levels of synaptopathy we found after blast in wild-type mice are consistent with changes found after noise exposure[4,17,30], and the lack of synaptopathy in Vglut3[KO] mice fit with previous reports after noise exposure[28]. Our new finding of mildly reduced synapse counts *Tecta*[C1509G/C1509G] mice at baseline is consistent with the concept that glutamate
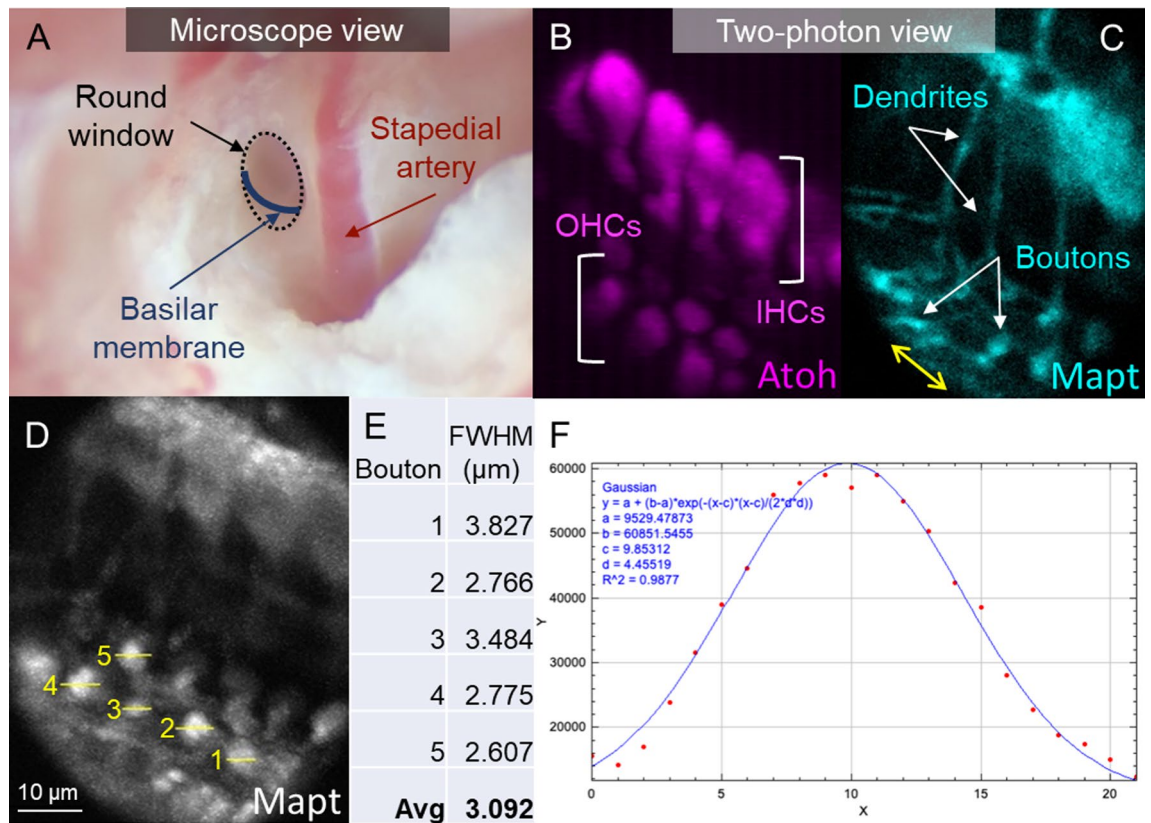
Fig. 8. In vivo imaging of the Atoh1$^{CreERT2-tdTomato}$;Tau^{EGFP} mouse through the round window allows visualization of synaptic boutons within the organ of Corti. (**A**) The microscopic view shows the orientation of the organ of Corti in relation to anatomic landmarks. (**B**) The inner hair cells (*IHCs*) and outer hair cells (*OHCs*) are depicted in magenta. (**C**) Nerve dendrites and boutons are depicted in cyan. The coursing of the dendrites longitudinally (yellow arrow) indicates that this image was taken at the bottom of the OHCs, where the type II afferents run. (**D**) Bouton size was quantified by selecting five boutons within the z-stack of a two-photon image. (**E,F**) The intensity was plotted for each point and fitted to a Gaussian curve. The full width at half maximum was recorded for each bouton and averaged.

contributes to synapse maintenance. *Tecta*$^{C1509G/C1509G}$ mice have reduced hair cell stimulation and elevated auditory thresholds, whereas Vglut3^{KO} are deaf[22,31].

Both presynaptic ribbons labeled with CtBP2 and postsynaptic densities labeled with Homer were quantified to analyze synapse loss following experimental exposures. Presynaptic ribbons of the CBA/CaJ mouse decreased significantly after blast exposure across all regions of the cochlea. Postsynaptic densities also decreased; however, only the basal section was statistically significant. This may be explained by the fact that noise exposure has the greatest effects in the basal regions of the cochlea[4,30]. Alternatively, this may be because the Homer stain has higher background labeling, even though it has been shown to label the postsynaptic density with as much accuracy as other common stains such as GluA2, PSD-95, and Shank[32].

In vivo two-photon live imaging of the mouse cochlea through the round window membrane is a novel technique. It allowed us to dynamically study morphological changes in the auditory nerve boutons after noise and osmotic challenge. To the best of our knowledge, this is the first time that dynamic changes in auditory neurons have been imaged non-invasively in vivo. Our studies were limited to the most basal section of the cochlea where the round window is located. Using other techniques, such as creating an imaging window in the otic capsule bone, a similar technique may be used to image the ~ 6–20 kHz region of the mouse cochlea[33]. Our data confirm and extend TEM studies demonstrating dendritic swelling mediated by glutamate excitotoxicity[34]. Furthermore, this approach opens the possibility of many future studies, for example, to study the development of cochlear synaptopathy over time with good spatial localization. In addition, as new ion and voltage-dependent fluorophores with high sensitivity become available, physiological changes in auditory neurons could be studied in vivo with this technique.

Arguably the most significant limitation of our approach was the fluorescent labeling of the Atoh1$^{CreERT2-tdTomato}$;Tau^{EGFP} mouse. The spiral ganglion contains 90–95% type I myelinated afferent nerves projecting to IHCs in an unbranched fashion[35]. Given that multiple type I afferents synapse with one IHC, labeling of the inner hair cell synapses was too abundant for individual synapses to be resolved on two-photon imaging. Therefore, type II afferents were selected for analysis since synapses are less redundant in the OHC
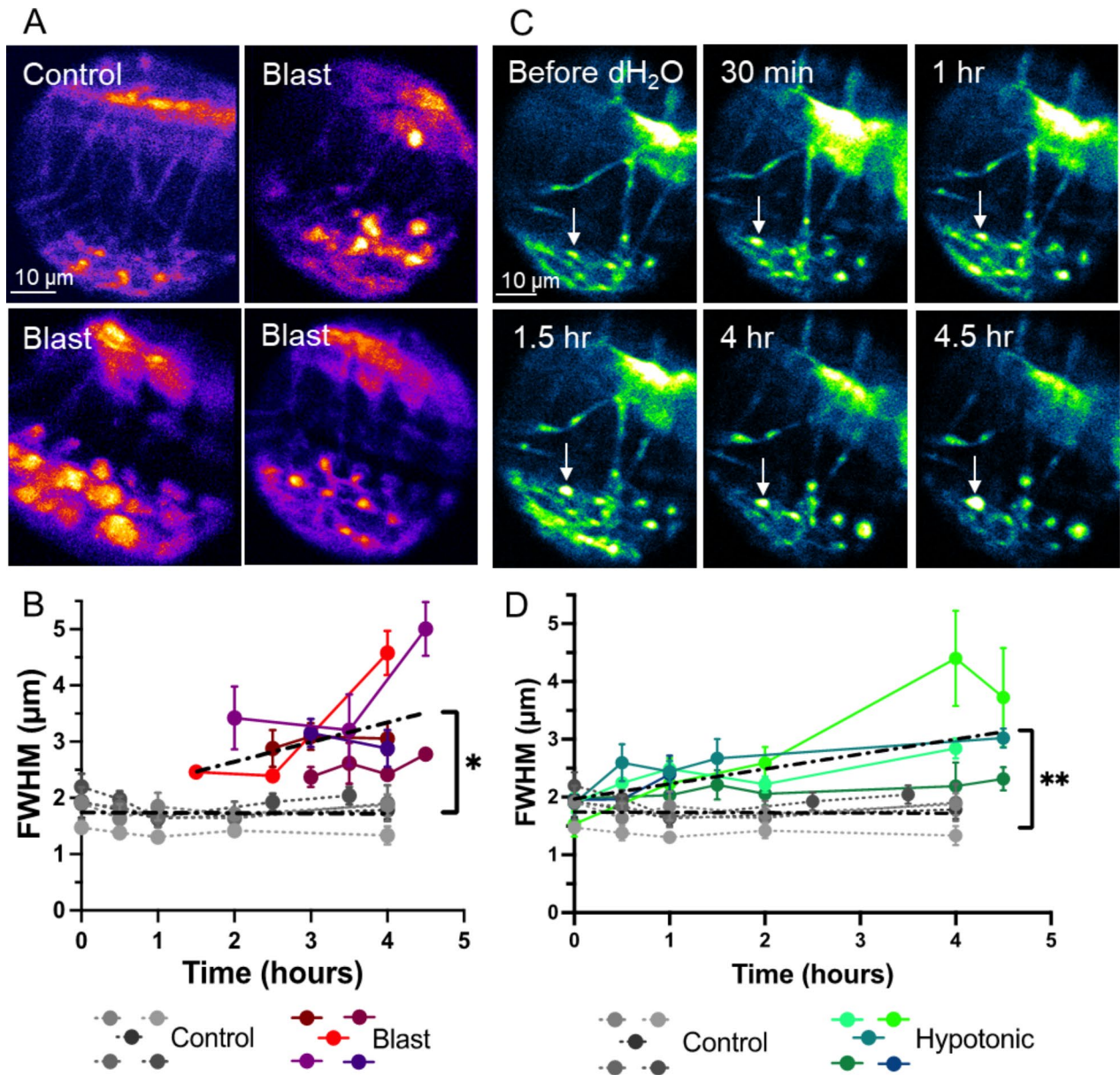
Fig. 9. Blast exposure and hypotonic challenge both produce bouton swelling in vivo. (**A**) Images from a control mouse and three different mice after blast. There is swelling of synaptic boutons after blast exposure. Only Mapt fluorescence is displayed with intensity pseudocolored. Bright yellow indicates high signal, violet is low signal. (**B**) Averaged data from control and blast-exposed mice. (**C**) Synaptic boutons also swell after hypotonic challenge, as documented from sequential images from one mouse. The swelling of one individual bouton over 4.5 h is highlighted (*arrow*). Only Mapt fluorescence is displayed with intensity pseudocolored. Bright yellow indicates high signal, blue is low signal. (**D**) Averaged data from control mice and mice exposed to the hypotonic challenge. *$p < 0.05$, **$p < 0.01$, $n = 5$. Error bars represent SEM.

region. Using a mouse model where the auditory nerve labeling is sparse would allow for direct analysis of the dendritic swelling under the IHCs.

Although it is well established that glutamate plays a major role in cochlear synaptopathy, the influence of other signaling molecules such as postsynaptic Ca^{2+} and extracellular K^+ must also be considered. The role of calcium-permeable AMPA-type glutamate receptors (CP-AMPAR) was tested and it was found that excess Ca^{2+} may underlie afferent terminal damage[36]. Elevation of extracellular K^+, a consequence of noise exposure, was found to cause dose-dependent IHC ribbon degeneration that could be reduced by BK channel blockers[37]. This study reports that IHC ribbons swelled but did not degenerate after the application of GluR agonists, suggesting that excess extracellular K^+ is the true mediator of IHC ribbon synapse degeneration[37]. Glutamate, Ca^{2+}, and K^+ most likely all contribute to cochlear synaptopathy, revealing multiple targets for potential prevention and treatment as we gain a better understanding of the mechanistic steps of cochlear synaptopathy.

This work, in combination with those of other labs, have now created a reasonably clear description of the mechanistic steps that cause endolymphatic hydrops and cochlear synaptopathy after noise trauma. In fact, these data provide a scientific basis for why patients with Meniere's disease have afferent neuronal loss beyond that predicted by their hair cell loss[38,39]. However, there is still a substantial amount of work to do to understand how to use this knowledge to help patients. After noise trauma, what is the best way to reduce the impact of glutamate excitotoxicity and within what time frame does this need to happen?

While the cause of Meniere's disease remains unknown, our data argue that something is upsetting the osmotic balance between the endolymph and perilymph. One intriguing possibility is that this is due to hair cell transduction channel block. Given the association between Meniere's disease and inflammation[40–42], there could be an inflammatory protein that enters the endolymph that has the right size and charge to plug the channel pore[43–48]. Despite these remaining questions, the significant movement in our understanding of the mechanisms of hearing loss is leading to successful treatments at the genetic level[49,50]. We are excited by the future possibilities for translating these findings into ways to help patients suffering from hearing loss.

Materials and methods
Animals/sex as a biological variable
All experiments were performed according to protocols approved by the Institutional Animal Care and Use Committee at the University of Southern California, and all methods were performed in accordance with the relevant guidelines and regulations. This study is reported in accordance with ARRIVE guidelines (https://arriveguidelines.org). Our study examined male and female animals, and similar findings are reported for both sexes. We used 51 CBA/CaJ (JAX#: 000654), 22 $Tecta^{C1509G/C1509G}$[23], and 38 Vglut3^{KO} (JAX#: 016931) mice of either sex aged 6–11 weeks. In addition, 15 Atoh1$^{CreERT2-tdTomato}$;Tau^{EGFP} of either sex aged 8–12 weeks were used for two-photon in vivo imaging. These mice were created by crossing the Atoh1CreERT2 mouse (JAX#: 007684) with an Ai14 Cre reporter strain (JAX#:007914), followed by another crossing with the Tau^{EGFP} mouse (JAX#:029219). The final result was the Atoh1$^{CreERT2-tdTomato}$;Tau^{EGFP} mouse that contains two fluorophores for separate identification of hair cells (*Atoh1*) and nerve fibers (microtubule-associated protein tau, *Mapt*). The mice were injected with Tamoxifen (Sigma) dissolved in corn oil (Sigma) at a concentration of 100 mg/kg on consecutive days P0 and P1. All mice were anesthetized using ketamine (100 mg/kg) and xylazine (10 mg/kg) for surgical procedures.

Blast exposure
Our custom-built blast chamber used to deliver blast waves to anesthetized mice has been previously described[51]. In short, compressed air was released down an elongated metal tube that sharpened the profile of the blast wave. Anesthetized mice were suspended in the tube within a pouch that shielded the body from the blast wave. Only the pinna protruded from the pouch so that the ears received the full impact of the blast wave. This permitted us to study the effect of the blast on the ear without systemic trauma. Mice were exposed to a blast wave with peak pressures between ~ 130 kPa (~ 196 dB SPL) and ~ 192 kPa (~ 200 dB SPL). Then, we either performed in vivo two-photon or OCT imaging or harvested the cochleae for confocal or TEM imaging.

Previously, we described the hair cell damage caused by this level of blast[16,51]. While there was no gross structural damage within the cochlea, nearly all OHCs within the basal 40% of the cochlea and some IHCs within the basal 20% were lost. There was also partial loss of auditory neurons within the spiral ganglion. While the peak pressure did vary a lot, the sound pressure of the exposure was fairly constant. We have shown that the level of cochlear damage is quite consistent within this range[51].

Hypotonic challenge
A hypotonic challenge was performed by applying distilled water (0 mOsm/kg) to the round window membrane of the mouse's right ear. The untreated left ear served as a control. Anesthetized mice underwent surgical dissection to expose the round window. Distilled water was applied directly to the round window membrane and filled the middle ear. This permitted osmosis to take place through this semipermeable membrane[52] into the cochlear perilymph. During this process, the mice were imaged in vivo either using OCT or two-photon fluorescence. During all experiments, the distilled water was exchanged every 15–30 min to maintain the osmotic gradient. To validate that these mice developed endolymphatic hydrops with this protocol, we imaged the cochlea through the ear canal.

For a different set of mice, a myringotomy was performed by puncturing a hole in the tympanic membrane of anesthetized mice. Distilled water was instilled to fill the middle ear space and cover the round window membrane. This hypotonic challenge was carried out for 5.5 h. After recovering from anesthesia, these mice were returned to the vivarium and sacrificed eight days later. The cochleae were collected for histological preparation and confocal imaging.

MET channel blocker and posterior semicircular canal injection
Wild-type CBA/CaJ mice were anesthetized, and surgery was performed to expose the left cochlea and posterior semicircular canal (PSCC). A 4 mM suspension of UoS-7692[46] (compound F5754-0139, Life Chemicals USA, Inc) in artificial perilymph (140 mM NaCl, 2 mM KCl, 2 mM MgCl2, 2 mM CaCl2, 20 mM HEPES with pH 7.4) containing 0.2% DMSO, 317 mOsm/kg was injected into the inner ear via the posterior semicircular canal (PSCC) injection technique as previously described[53,54]. Briefly, a canalostomy was made in the PSCC with the tip of a 28-gauge needle. A 110 μm polyimide tubing (MicroLumen, Oldsmar, FL) attached to 280 μm polyethylene tubing (SIMS Portex Ltd., UK) on a 10 μL Hamilton gastight syringe was loaded with injection solution. The injection tubing was inserted into the PSCC, and the tubing and canalostomy were sealed with histoacryl glue (Tissue Seal, LLC, Ann Arbor, MI). 1 μL of solution was injected using a syringe pump at 0.5 μL/min, and

another 1–2 injections of 0.5 – 1 µL volume were delivered 60–90 min after the initial injection to increase the concentration of compound delivered and minimize injection volume and pressure at a single time point.

Sound stimuli for vibrometry measurements were delivered in an open field configuration using an Etymotic ER2SE earbud and consisted of pure tones with a frequency ranging from 0.5 to 15 kHz in 0.5 kHz steps and a level ranging from 10 to 80 dB SPL in 10 dB steps. Each stimulus duration was 100 ms. Basilar membrane vibrometry measurements were taken at baseline following surgical opening of the bulla, after performing a posterior semicircular canalostomy and inserting tubing containing injection solution, following injection of the perfusate for up to 300 min, and immediately following euthanasia of the mouse at the conclusion of the experiment. The characteristic frequency (CF) was identified as the frequency with the largest vibratory response to the lowest stimulus intensity that produced a vibratory response above the noise floor. Cochlear gain was calculated as the difference in vibratory sensitivity (displacement normalized to the sound intensity) to 80- and 30-dB SPL stimuli at the CF. The gain and CF were recorded prior to (0 min), after PSCC injection of the solution (at approximately 90 min, 180 min, 300 min), and after euthanasia of the mouse. To ensure the 0.2% DMSO was not contributing to endolymphatic hydrops and vibrometry changes, a 0.2% DMSO in artificial perilymph solution without UoS-7692 but with the same osmolality was injected via the same PSCC technique in CBA/CaJ mice as a control. All vibrometry experiments were carried out on the left ear.

Histological preparation and immunofluorescence

Our methods of histological preparation and immunofluorescence have been previously reported[15]. Eight days after CBA/CaJ, *Tecta*^C1509G/C1509G, and Vglut3^KO mice were exposed to a blast wave, hypotonic challenge, or no exposure, the mice were euthanized, and their cochleae extracted.

Tissue fixation was performed by opening a fenestra in the cochlear apex and perfusing 4% paraformaldehyde through the round window then immersing the cochlea in 4% paraformaldehyde for 30 min. The cochlea was decalcified by immersing it in a 0.5 M EDTA solution (pH 8) for 6 h at room temperature, then washing it in PBS. Then the cochlear sensory epithelium was dissected into apex, middle, and base sections. These sections approximately correlate to the frequency range of $5-11.5$ kHz, 11.5–26 kHz, and 26–60 kHz according to a previously established tonotopic cochlear place-frequency map[55]. Approximately $10 \pm 5\%$ of the cochlea hook region was damaged due to dissection limitation and not studied.

Following dissection, cochlear tissues were incubated in blocking solution (5% goat serum, 0.1% Triton X-100, and 1.0% BSA in PBS) at room temperature for 1 h. Tissue samples were then incubated with primary antibodies diluted in the same blocking solution for 2 days at 4 °C followed by 2 h at 37 °C. The primary antibodies included Mouse anti-CtBP2 IgG1 (1:200; BD Biosciences, 612,004), Rabbit anti-Homer1 polyclonal (1:800; Synaptic Systems, 160 003), and Mouse anti-Myosin VI (A-9) IgG3 (1:100; Santa Cruz Biotechnology, sc-393558). The tissues were washed in PBST (0.1% Triton X-100 in PBS) and then incubated with a secondary antibody solution diluted in 0.1% Triton X-100 and 0.1% BSA in PBS for 1 h at room temperature. The secondary antibodies were conjugated with Goat anti-Mouse IgG3 Alexa Fluor 488 (1:500; Invitrogen, A-21151), Goat anti-Rabbit IgG (H + L) Alexa Fluor 555 (1:500; Invitrogen, A-21428), Goat anti-Mouse IgG1 Alexa Fluor 647 (1:500; Invitrogen, A-21240), and Alexa Fluor 405 Phalloidin (1:200; Invitrogen, A30104). Following incubation, the tissues were washed in PBS with 1:4000 Alexa Fluor 405 phalloidin. Then the tissues were mounted on glass slides using Fluoromount-G Mounting Medium with DAPI (Invitrogen, 00-4959-52). Slides were stored overnight at 4 °C before confocal imaging.

Confocal imaging

Immunostained cochlear tissue slides were imaged using an inverted confocal microscope (Leica SP8). A 20x (0.75 N.A.) or 25x (0.95 N.A.) objective was first used to obtain an overview image and check tissue integrity. Then, high-resolution images were captured using a 63 × objective (1.4 N.A.), with a z-step of 0.15 µm. The images were deconvolved in either Huygens Essential or Leica's Lightning software using the default deconvolution algorithm. For each 63 × image, the number of inner hair cells (IHCs), CtBP2-labeled presynaptic ribbons, and Homer-labeled postsynaptic densities (PSDs) were counted automatically using Imaris software (Version 9.9, Oxford Instruments), which applies a thresholding and background subtraction algorithm. All automated counts were verified by eye, and manual adjustments were performed if needed to improve the accuracy of the counts.

TEM

Mice cochleae were exposed to a blast wave and prepared for TEM according to the protocol previously described (Gratton et al., 2005). Anesthetized control and blast-exposed cochleae were fixed at ~ 3 h, ~ 7 h, and ~ 24 h post-blast via perfusion of the fixative (1% OsFeCN and 1% Paraformaldehyde 4 in 0.1 M sodium cacodylate buffer) through the oval window. The bulla was immersed in fixative (12 h, 4 °C), rinsed in the buffer, and shipped to Washington University in St Louis for further processing and imaging. In the Gratton lab, the cochlea underwent *en bloc* post-staining with 1% uranyl acetate (UA) and Walton's lead aspartate to enhance contrast. The cochleae were decalcified (120 mM EDTA, 23 °C), dehydrated, and embedded in epoxy resin (Embed 812, EMS, Hatfield, PA). The cochleae were bisected along the modiolus and re-embedded. The polymerized cochleae were bisected in the mid-modiolar plane. Following re-embedding, modiolar cochlear Sects. (70 nm) were cut and mounted on copper hex grids. Images from the upper basal turn (approx. 28–32 kHz) were collected and archived using a JEOL 1200 EX transmission electron microscope (JEOL USA Inc., Peabody, MA) equipped with an AMT 8-megapixel digital camera and AMT Image Capture Engine V602 software (Advanced Microscopy Techniques, Woburn, MA). Final figures were assembled using Adobe Photoshop and Illustrator software (Adobe Systems).

In vivo OCT imaging

Following surgical dissection, anesthetized mice were positioned on our custom-built OCT system, which has previously been described[56]. With this approach, we imaged the apical cochlear turn about a half turn down from the helicotrema, which is roughly the 9 kHz region[56–58]. For the hypotonic challenge experiments, cochleae were imaged at 0, 30, and 60 min after initiation of the hypotonic challenge. For the MET channel blockade experiments, OCT images were captured at baseline and up to 300 min following injection of UoS-7692 via the posterior semicircular canal. Cross-sectional images were analyzed in ImageJ (Version 2.9.0, National Institutes of Health).

In vivo two-photon imaging

Atoh1$^{CreERT2-tdTomato}$;Tau^{EGFP} mice were used for in vivo two-photon imaging because the hair cells contain tdTomato and the neurons contain GFP. Under anesthesia, the mouse middle ear bulla was surgically opened to expose the round window and the mouse was placed on our custom-built two-photon imaging system. We imaged non-invasively through the round window membrane.

Two-photon excitation was accomplished by scanning a 150-mW femtosecond pulsed laser at 950 nm (Chameleon Ultra II, Coherent) across the sample through a 40x (0.8 NA) water immersion objective lens on a custom-built microscope. Fluorescence from the sample was collected through the objective and separated from the excitation beam path with a long-pass dichroic mirror with a cutoff wavelength of 735 nm. The red and green fluorescence channels were separated using another long-pass dichroic mirror with a cutoff wavelength of 585 nm. A final filter was added to the green channel that further reduced the spectrum of green fluorescence to a bandwidth of 40 nm centered at 500 nm. The detectors used in both channels were hybrid photodetectors (R11322U-40, Hamamatsu) with variable gain settings that allowed control of relative brightness between the fluorescence detected from the two channels.

Two-photon images were acquired with customized software. The field of view was 60 μm in diameter. Volumes were acquired using 1 μm steps in the z direction for a total of 50 steps. Images were imported into ImageJ. Synapses at the base of the outer hair cells (OHCs) were identified to study the type II afferent auditory nerve fibers, as opposed to the medial olivocochlear bundle efferent fibers, which are higher up on the side of the OHCs. From each mouse, five individual boutons from one imaging position were selected for analysis. Whenever possible, the same five boutons were analyzed across the complete time course for a given mouse. We used an open-source full width at half maximum ImageJ macro plug-in that utilized ImageJ's innate algorithms to fit the intensity profile of each synaptic bouton to a Gaussian curve and calculate the width at half the height.

Statistical analysis

All statistical analysis was performed using GraphPad Prism (Version 9.4.1, GraphPad Software). The two-tailed non-paired t-test was used to assess for differences in endolymph volume, as measured by SM/SV ratio, between control and blast-exposed mice. Change in SM/SV ratio over time after application of a MET channel blocker or hypotonic challenge was compared using a two-tailed paired t-test. A comparison of gain and BF measurements following PSCC injection of solution was also made using a two-tailed paired t-test. Confocal imaging counts of presynaptic ribbons, postsynaptic densities, and IHCs across different exposure groups were analyzed using a two-way ANOVA with a post-hoc Tukey multiple comparisons test. For two-photon data, a linear regression was fit to the dataset to quantify the change in dendritic swelling following hypotonic challenge or blast exposure. Analysis of covariance was used to determine if the linear regression lines of the control and experimental groups were statistically different. All box and whisker graphs show a box extending from the 25th to 75th percentiles with a line in the middle of the box plotted at the median. The whiskers represent minimum and maximum values. Statistical results presented include t-values and degrees of freedom for t-tests and F values and degrees of freedom for ANOVAs. For all analyses, a p-value < 0.05 was considered statistically significant. Also, we independently compared males and females within each cohort for every statistical test to assess for sex differences. There were no statistically significant sex differences in the effects. Thus, males and females were combined for the presented results.

Data availability

Data supporting the findings of this study will be shared upon request by emailing the senior author at oghalai@usc.edu. We also have uploaded key datasets to our GitHub site[59].

References

1. Shargorodsky, J. et al. Change in prevalence of hearing loss in US adolescents. *JAMA* **304**, 772. https://doi.org/10.1001/jama.2010.1124 (2010).
2. Furness, D. N. Molecular basis of hair cell loss. *Cell Tissue Res.* **361**, 387–399. https://doi.org/10.1007/s00441-015-2113-z (2015).
3. Yang, C. H., Schrepfer, T. & Schacht, J. Age-related hearing impairment and the triad of acquired hearing loss. *Front. Cell Neurosci.* https://doi.org/10.3389/FNCEL.2015.00276 (2015).
4. Liberman, M. C. & Kujawa, S. G. Cochlear synaptopathy in acquired sensorineural hearing loss: Manifestations and mechanisms. *Hear. Res.* **349**, 138–147. https://doi.org/10.1016/J.HEARES.2017.01.003 (2017).
5. Mammano, F. et al. ATP-Induced Ca(2+) release in cochlear outer hair cells: Localization of an inositol triphosphate-gated Ca(2+) store to the base of the sensory hair bundle. *J. Neurosci.* **19**, 6918–6929 (1999).
6. Piazza, V., Ciubotaru, C. D., Gale, J. E. & Mammano, F. Purinergic signalling and intercellular Ca2+ wave propagation in the organ of Corti. *Cell Calcium* **41**, 77–86. https://doi.org/10.1016/j.ceca.2006.05.005 (2007).

7. Pujol, R. & Puel, J. L. Excitotoxicity, synaptic repair, and functional recovery in the mammalian cochlea: A review of recent findings. *Ann. N.Y. Acad. Sci.* **884**, 249–254. https://doi.org/10.1111/j.1749-6632.1999.tb08646.x (1999).

8. Mayer, M. L. & Westbrook, G. L. Cellular mechanisms underlying excitotoxicity. *Trends Neurosci.* **10**, 59–61. https://doi.org/10.1016/0166-2236(87)90023-3 (1987).

9. Choi, D. W. & Rothman, S. M. The role of glutamate neurotoxicity in hypoxic–ischemic neuronal death. *Annu. Rev. Neurosci.* **13**, 171–182. https://doi.org/10.1146/annurev.ne.13.030190.001131 (1990).

10. Kujawa, S. G. & Liberman, M. C. Adding insult to injury: Cochlear nerve degeneration after "temporary" noise-induced hearing loss. *J. Neurosci.* **29**, 14077–14085. https://doi.org/10.1523/JNEUROSCI.2845-09.2009 (2009).

11. Moser, T. & Starr, A. Auditory neuropathy—Neural and synaptic mechanisms. *Nat. Rev. Neurol.* **12**, 135–149. https://doi.org/10.1038/nrneurol.2016.10 (2016).

12. Lin, H. W., Furman, A. C., Kujawa, S. G. & Liberman, M. C. Primary neural degeneration in the guinea pig cochlea after reversible noise-induced threshold shift. *J. Assoc. Res. Otolaryngol.* https://doi.org/10.1007/s10162-011-0277-0 (2011).

13. Schaette, R. & McAlpine, D. Tinnitus with a normal audiogram: Physiological evidence for hidden hearing loss and computational model. *J. Neurosci.* **31**, 13452–13457. https://doi.org/10.1523/JNEUROSCI.2156-11.2011 (2011).

14. Kohrman, D. C., Wan, G., Cassinotti, L. & Corfas, G. Hidden hearing loss: A disorder with multiple etiologies and mechanisms. *Cold Spring Harb. Perspect. Med.* https://doi.org/10.1101/CSHPERSPECT.A035493 (2020).

15. Kim, J., Xia, A., Grillet, N., Applegate, B. E. & Oghalai, J. S. Osmotic stabilization prevents cochlear synaptopathy after blast trauma. *Proc. Natl. Acad. Sci.* https://doi.org/10.1073/pnas.1720121115 (2018).

16. Paik, C. B., Pei, M. & Oghalai, J. S. Review of blast noise and the auditory system. *Hear Res.* https://doi.org/10.1016/J.HEARES.2022.108459 (2022).

17. Badash, I. et al. Endolymphatic hydrops is a marker of synaptopathy following traumatic noise exposure. *Front. Cell Dev. Biol.* **9**, 747870 (2021).

18. Liao, Y. H. & Young, Y. H. Predicting secondary endolymphatic hydrops in patients with noise-induced hearing loss. *Acta Otolaryngol.* **142**, 161–167. https://doi.org/10.1080/00016489.2022.2037703 (2022).

19. Zhang, W. et al. The correlation between endolymphatic hydrops and clinical features of meniere disease. *Laryngoscope* **131**, E144–E150. https://doi.org/10.1002/LARY.28576 (2021).

20. Sun, Q. et al. Quantification of endolymphatic hydrops and its correlation with Meniere's disease clinical features. *Clin. Otolaryngol.* **46**, 1354–1361. https://doi.org/10.1111/COA.13847 (2021).

21. Gueta, R. et al. Structural and mechanical analysis of tectorial membrane Tecta mutants. *Biophys. J.* **100**, 2530–2538. https://doi.org/10.1016/J.BPJ.2011.04.024 (2011).

22. Liu, C. C. et al. Biophysical mechanisms underlying outer hair cell loss associated with a shortened tectorial membrane. *J. Assoc. Res. Otolaryngol.* **12**, 577–594. https://doi.org/10.1007/S10162-011-0269-0 (2011).

23. Xia, A. et al. Deficient forward transduction and enhanced reverse transduction in the alpha tectorin C1509G human hearing loss mutation. *Dis. Model Mech.* **3**, 209–223. https://doi.org/10.1242/dmm.004135 (2010).

24. Akil, O. et al. Restoration of hearing in the VGLUT3 knockout mouse using virally mediated gene therapy. *Neuron* **75**, 283–293. https://doi.org/10.1016/j.neuron.2012.05.019 (2012).

25. Ruel, J. et al. Impairment of SLC17A8 encoding vesicular glutamate transporter-3, VGLUT3, underlies nonsyndromic deafness DFNA25 and inner hair cell dysfunction in null mice. *Am. J. Hum. Genet.* **83**, 278–292. https://doi.org/10.1016/J.AJHG.2008.07.008 (2008).

26. Choi, C.-H. & Oghalai, J. S. Perilymph osmolality modulates cochlear function. *Laryngoscope* **118**, 1621–1629. https://doi.org/10.1097/MLG.0b013e3181788d72 (2008).

27. Seal, R. P. et al. Sensorineural deafness and seizures in mice lacking vesicular glutamate transporter 3. *Neuron* **57**, 263–275. https://doi.org/10.1016/J.NEURON.2007.11.032 (2008).

28. Kim, K. X. et al. Vesicular glutamatergic transmission in noise-induced loss and repair of cochlear ribbon synapses. *J. Neurosci.* **39**, 4434–4447. https://doi.org/10.1523/JNEUROSCI.2228-18.2019 (2019).

29. Berglund, A. M. & Ryugo, D. K. Hair cell innervation by spiral ganglion neurons in the mouse. *J. Comput. Neurol.* **255**, 560–570. https://doi.org/10.1002/cne.902550408 (1987).

30. Liberman, L. D. & Liberman, M. C. Dynamics of cochlear synaptopathy after acoustic overexposure. *J. Assoc. Res. Otolaryngol.* **16**, 205–219. https://doi.org/10.1007/S10162-015-0510-3 (2015).

31. Akil, O. et al. Restoration of hearing in the VGLUT3 knockout mouse using virally-mediated gene therapy. *Neuron* **75**, 283–293. https://doi.org/10.1016/j.neuron.2012.05.019 (2012).

32. Martinez-Monedero, R. et al. GluA2-containing AMPA receptors distinguish ribbon-associated from ribbonless afferent contacts on rat cochlear hair cells. *eNeuro* https://doi.org/10.1523/ENEURO.0078-16.2016 (2016).

33. Kim, J. & Ricci, A. J. A chemo-mechanical cochleostomy preserves hearing for the in vivo functional imaging of cochlear cells. *Nat. Protoc.* **18**, 1137–1154. https://doi.org/10.1038/s41596-022-00786-4 (2023).

34. Ruel, J. et al. Physiology, pharmacology and plasticity at the inner hair cell synaptic complex. *Hear Res.* **227**, 19–27. https://doi.org/10.1016/j.hears.2006.08.017 (2007).

35. Spoendlin, H. Anatomy of cochlear innervation. *Am. J. Otolaryngol.* **6**, 453–467. https://doi.org/10.1016/s0196-0709(85)80026-0 (1985).

36. Sebe, J. Y. et al. Ca2+-permeable AMPARs mediate glutamatergic transmission and excitotoxic damage at the hair cell ribbon synapse. *J. Neurosci.* **37**, 6162–6175. https://doi.org/10.1523/JNEUROSCI.3644-16.2017 (2017).

37. Zhao, H.-B., Zhu, Y. & Liu, L.-M. Excess extracellular K+ causes inner hair cell ribbon synapse degeneration. *Commun. Biol.* **4**, 24. https://doi.org/10.1038/s42003-020-01532-w (2021).

38. Nadol, J. B. Jr. & Thornton, A. R. Ultrastructural findings in a case of Meniere's disease. *Ann. Otol. Rhinol. Laryngol.* **96**, 449–454 (1987).

39. Momin, S. R., Melki, S. J., Alagramam, K. N. & Megerian, C. A. Spiral ganglion loss outpaces inner hair cell loss in endolymphatic hydrops. *Laryngoscope* **120**, 159–165. https://doi.org/10.1002/lary.20673 (2010).

40. Frejo, L. & Lopez-Escamez, J. A. Cytokines and inflammation in meniere disease. *Clin. Exp. Otorhinolaryngol.* **15**, 49–59. https://doi.org/10.21053/CEO.2021.00920 (2022).

41. Sekulic, M., Puche, R., Bodmer, D. & Petkovic, V. Human blood-labyrinth barrier model to study the effects of cytokines and inflammation. *Front. Mol. Neurosci.* https://doi.org/10.3389/FNMOL.2023.1243370 (2023).

42. Xie, S. T., Zhang, R. F., Tang, Y. R. & Dai, Q. Q. Exploring causal correlations between inflammatory cytokines and Ménière's disease: A Mendelian randomization. *Front. Immunol.* https://doi.org/10.3389/FIMMU.2024.1373723 (2024).

43. Kim, J., Hemachandran, S., Cheng, A. G. & Ricci, A. J. Identifying targets to prevent aminoglycoside ototoxicity. *Mol. Cell. Neurosci.* https://doi.org/10.1016/j.mcn.2022.103722 (2022).

44. Huth, M. E., Ricci, A. J. & Cheng, A. G. Mechanisms of aminoglycoside ototoxicity and targets of hair cell protection. *Int. J. Otolaryngol.* **2011**, 937861. https://doi.org/10.1155/2011/937861 (2011).

45. Kitcher, S. R. et al. ORC-13661 protects sensory hair cells from aminoglycoside and cisplatin ototoxicity. *JCI Insight* https://doi.org/10.1172/JCI.INSIGHT.126764 (2019).

46. Kenyon, E. J. et al. Identification of a series of hair-cell MET channel blockers that protect against aminoglycoside-induced ototoxicity. *JCI Insight* https://doi.org/10.1172/JCI.INSIGHT.145704 (2021).

47. Kim, J., Hemachandran, S., Cheng, A. G. & Ricci, A. J. Identifying targets to prevent aminoglycoside ototoxicity. *Mol. Cell Neurosci.* https://doi.org/10.1016/J.MCN.2022.103722 (2022).
48. Huth, M. E. et al. Designer aminoglycosides prevent cochlear hair cell loss and hearing loss. *J. Clin. Invest.* **125**, 583–592. https://doi.org/10.1172/JCI77424 (2015).
49. Lv, J. et al. AAV1-hOTOF gene therapy for autosomal recessive deafness 9: A single-arm trial. *Lancet* https://doi.org/10.1016/S0140-6736(23)02874-X (2024).
50. Jiang, L., Wang, D., He, Y. & Shu, Y. Advances in gene therapy hold promise for treating hereditary hearing loss. *Mol. Ther.* **31**, 934–950. https://doi.org/10.1016/J.YMTHE.2023.02.001 (2023).
51. Cho, S.-I. et al. Mechanisms of hearing loss after blast injury to the ear. *PLoS ONE* **8**, e67618. https://doi.org/10.1371/journal.pone.0067618 (2013).
52. Stevens, S. M., Brown, L. S. N., Ezell, P. C. & Lang, H. The mouse round-window approach for ototoxic agent delivery: A rapid and reliable technique for inducing cochlear cell degeneration. *J. Vis. Exp.* https://doi.org/10.3791/53131 (2015).
53. Guo, J. Y. et al. Canalostomy as a surgical approach to local drug delivery into the inner ears of adult and neonatal mice. *J. Vis. Exp.* https://doi.org/10.3791/57351 (2018).
54. Kim, J. & Ricci, A. J. In vivo real-time imaging reveals megalin as the aminoglycoside gentamicin transporter into cochlea whose inhibition is otoprotective. *Proc. Natl. Acad. Sci. U.S.A.* **119**, e2117946119. https://doi.org/10.1073/PNAS.2117946119/SUPPL_FILE/PNAS.2117946119.SM04.MOV (2022).
55. Müller, M., von Hünerbein, K., Hoidis, S. & Smolders, J. W. T. A physiological place-frequency map of the cochlea in the CBA/J mouse. *Hear Res.* **202**, 63–73. https://doi.org/10.1016/j.heares.2004.08.011 (2005).
56. Dewey, J. B., Applegate, B. E. & Oghalai, J. S. Amplification and suppression of traveling waves along the mouse organ of Corti: Evidence for spatial variation in the longitudinal coupling of outer hair cell-generated forces. *J. Neurosci.* **39**, 1805–1816. https://doi.org/10.1523/JNEUROSCI.2608-18.2019 (2019).
57. Gao, S. S. et al. Vibration of the organ of Corti within the cochlear apex in mice. *J. Neurophysiol.* **112**, 1192–1204. https://doi.org/10.1152/jn.00306.2014 (2014).
58. Lee, H. Y. et al. Noninvasive in vivo imaging reveals differences between tectorial membrane and basilar membrane traveling waves in the mouse cochlea. *Proc. Natl. Acad. Sci. U.S.A.* **112**, 3128–3133. https://doi.org/10.1073/pnas.1500038112 (2015).
59. Oghalai, J.S. GitHub repository (2023). https://github.com/jso111/. https://github.com/jso111/.

Acknowledgements

Author contributions

PMQ, BEA, MAG, and JSO designed research. BEA, CBW, and JSO developed the hardware to perform the experiments. MJS developed the software to perform the experiments. MLF, CBP, PMQ, DWP, JW, GWP, and MAG performed the experiments. MLF, CBP, PMQ, DWP, MAG, MJS, and JSO analyzed the data. MLF, CBP, DWP, CBW, MAG, and JSO wrote the paper. All authors reviewed the manuscript.

Declarations

Competing interests

John Oghalai and Brian Applegate are founders of AO technologies, with the goal of translating inner ear imaging technologies for clinical purposes. The other authors have no competing interests.

Additional information

Supplementary Information The online version contains supplementary material available at https://doi.org/10.1038/s41598-024-77154-7.

Correspondence and requests for materials should be addressed to J.S.O.

Reprints and permissions information is available at www.nature.com/reprints.

Publisher's note Springer Nature remains neutral with regard to jurisdictional claims in published maps and institutional affiliations.